Ionospheric Scintillation Awareness for GPS and Other Constellations by Probability Maps

André Ricardo Fazanaro Martinon, Stephan Stephany, Eurico Rodrigues de Paula

Instituto Nacional de Pesquisas Espaciais (INPE)
Av. dos Astronautas, 1758, CEP 12227-010, São José dos Campos SP, Brazil

{andre.martinon,stephan.stephany,eurico.paula}@inpe.br

Abstract. *Ionospheric scintillation may disturb radio-frequency signals and other electromagnetic waves. In the case of Global Navigation Satellite Systems, strong scintillation can cause loss-of-lock between satellite and ground receiver, and thus positioning errors. Remote sensing satellites can also be affected, generating distorted images. Scintillation maps covering the globe are available, but refer to the vertical projection of the scintillation, while satellite signals are emitted or received at an angle in the majority of the cases. Therefore, this work proposes the use of probability maps, generated from standard scintillation maps, in order to assess the risk of undergoing scintillation according to the satellite orbit.*

1. Introduction

This work proposes the innovative scintillation probability map for evaluating if the satellite-ground station links of a Global Navigation Satellite System (GNSS) like GPS can be affected by strong ionospheric scintillation, causing loss-of-lock or positioning error. Scintillation maps covering the globe are normally available in near real time, yielding the vertical projection of the amplitude scintillation index S4 at every grid point with a given time resolution. These maps are intended to be a representation of scintillation in the ionosphere. However, considering the scintillation map for a particular time interval, a GNSS receiver at a given latitude and longitude will not experience scintillation effects corresponding to its location, since the azimuth and elevation angles of each satellite-receiver link must be taken into account. Therefore, such scintillation probability maps are proposed, which provide for every grid point a probability of a receiver undergoing scintillation in function of the average positions of the set of GNSS satellites within reach in the considered time interval. Satellite positions can be promptly estimated from IGS (International GNSS Service) "Precise Satellites Orbits" data, describing the satellite orbits. Consequently, neighboring scintillation occurrences are taken into account in the probability map, providing to GNSS users a better insight about the possibility of being affected by strong scintillation near or at their position.

These newly proposed probability maps are made from different scintillation maps covering most of South America, which are more precise than standard maps due to a better interpolation algorithm and pre-processing schemes [Martinon et al., 2022], but the latter could also be employed. Typically, the S4 index is estimated from radio signals acquired at 50 Hz during a 1-minute period, yielding a S4 value given by the standard deviation of the signal intensity normalized by its mean [Van Dierendonck et al., 1993]. These values are calculated for each GNSS satellite-station link using the GNSS constellations currently available (GPS and others) providing compatibility even between stations that use different receivers [de Paula et al., 2021]. The present work employs only the GPS constellation to produce the scintillation and then the probability maps. It is expected that the proposed ionospheric scintillation probability maps will provide warnings for users of GNSS-based applications, including aerial navigation, ADS-B (Automatic Dependent Surveillance–Broadcast), takeoff and landing

procedures, precision agriculture, and positioning of offshore oil prospecting platforms. In addition, these maps can be assimilated by ionospheric models and/or used in scintillation research, besides being included as part of the monitoring services provided by the Brazilian Airspace Control System (SISCEAB).

The probability maps presented here are specific for GNSS applications, but the same approach can be easily adapted for remote sensing satellites, by taking into account the scan angle to nadir for each swath of the considered onboard sensor. The same scintillation map may then be employed to generate customized probability maps, according to the remote sensing satellite orbit and scan angle. Besides radio-frequency, some other electromagnetic waves may be affected by scintillation, as in the case of SAR (Synthetic Aperture Radar). On the other hand, distortions in SAR images caused by scintillation may allow to identify ionospheric bubbles [Sato et al., 2021], large structures of depleted plasma that contain high density gradients associated with the occurrence of scintillation.

2. Ionospheric Scintillation Maps Generation

The ionospheric scintillation maps used in this work were generated using S4 index data of GPS receivers covering most of South America, and provided by the GNSS stations of two networks, LISN (Low-Latitude Ionospheric Sensor Network) [Valladares and Chau 2012] and INCT GNSS-NavAer [Vani et al., 2017]. The data collected by each receiver of the monitoring station includes the GPS satellite positions (azimuth and elevation) and the corresponding ionospheric scintillation indexes S4.

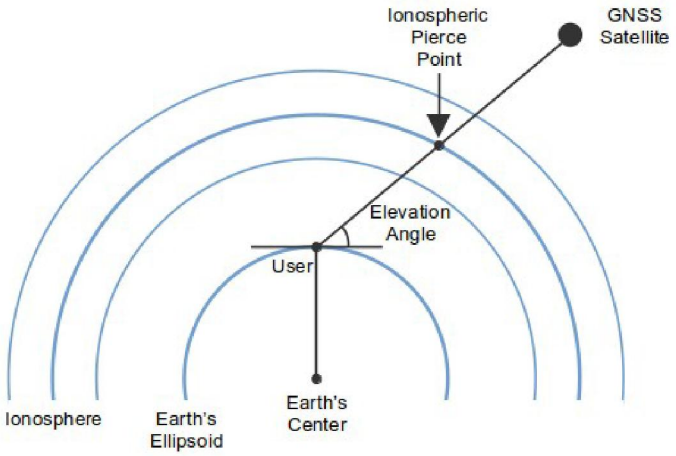

Figure 1. Geometry of a satellite-ground station line-of-sight depicting the Ionospheric Pierce Point

The making of a scintillation map covering a time interval (here, 15-minute) requires some assumptions/steps: (i) the ionosphere is modeled as a thin spherical shell over the Earth at the mean altitude of 350 km, which corresponds to the maximum observed TEC (Total Electron Content); (ii) for each satellite-receiver link, the position of a Ionospheric Pierce Point (IPP, shown in Figure 1) can be obtained as the intersection of the line-of-sight receiver-satellite with the ionosphere, using the receiver coordinates and azimuth and elevation angles of the satellite [Prol et al., 2017]; (iii) each line-of-sight satellite-receiver is a slant path, i.e. the GNSS signal traverses a longer path inside ionospheric irregularities than for a vertical path, depending on the elevation angle; a way to normalize S4 values of observations with different elevation angles is to project each value to the vertical direction, assuming a line-of-sight of 90° at the IPP [Spogli et al., 2009 and 2013]; (iv) considering a 1.0°x1.0° resolution grid, the IPPs are grouped into the corresponding cells, and the S4 value for each cell is given

by the corresponding S4 values of the IPPs reduced by the maximum value, mean value or mean value of the 3rd quartile; (v) the interpolation of the cell S4 values yields the scintillation map, covering in this work, longitudes in the range -78.0° to -30.0°, and latitudes -39.0° to 9.0°, both with a 0.25° resolution. Differently from standard methods like Inverse Distance Weighting [Rezende et al., 2007], interpolation is performed using Gaussian Process Regression with a specific kernel, and adopting the Haversine distance as the distance metric. Figure 2 shows the resulting 15-minute scintillation map for October 10, 2014 at 00:31 UTC time, using S4 values projected to the vertical, and reducing the cell grouped IPPs by the mean of the 3rd quartile of their S4 values.

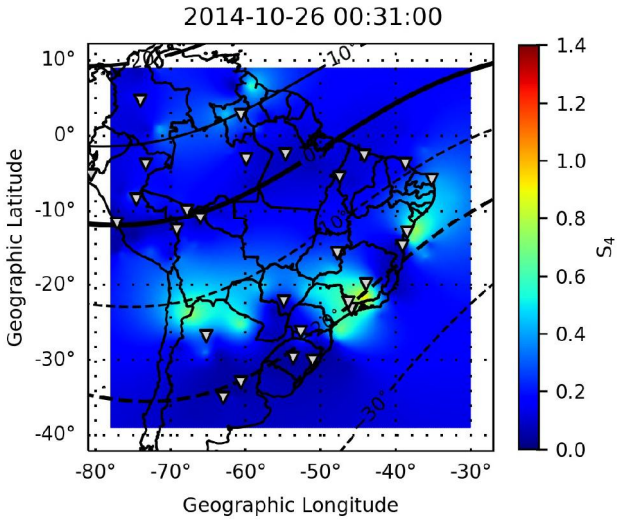

Figure 2. Example of a scintillation map, where color scale refers to S4 values. Curved lines depict magnetic latitudes, and triangles show GPS stations.

3. Proposed Methodology for Scintillation Probability Maps

This work proposes for the first time the making of scintillation probability maps, which are derived from the scintillation maps for the corresponding area and time interval. Such a map provides for a receiver location the probability of undergoing scintillation, specifically strong scintillation (S4 above 0.70), though it can be extended for any other scintillation level, like null [0.00-0.15], weak (0.15-0.30], or moderate (0.30-0.70]. A GPS user may consult scintillation probability maps, which can be generated in real time, in order to mitigate consequences of a possible loss of lock during position assessment or navigation.

This probability is calculated for every grid point of the map retrieving the S4 values of nearby points in the scintillation map, defined using the positions of the set of in-range GPS satellites with elevation angle higher than 30°, and thus take into account the influence of the elevation and azimuthal angles of the line-of-sight satellite-station for a hypothetical station at the grid point. Each GPS satellite position can be calculated by the available IGS satellite orbit data. The hypothetical GPS receiver is assumed as locking up to all satellites in its vicinity, thus defining a set of surrounding IPPs, each one with a S4 value obtained from the corresponding scintillation map interpolating the S4 values of the four closest neighboring grid points. The probability at the grid point is then simply given by the ratio of IPPs with strong scintillation (or any other level) and the total number of IPPs. The latter number varies according to the grid point latitude, decreasing as the latitude increases. Figure 3 shows the resulting 15-minute strong scintillation probability map for October 10, 2014 at 00:31 UTC time derived from the corresponding scintillation map shown in Figure 2.

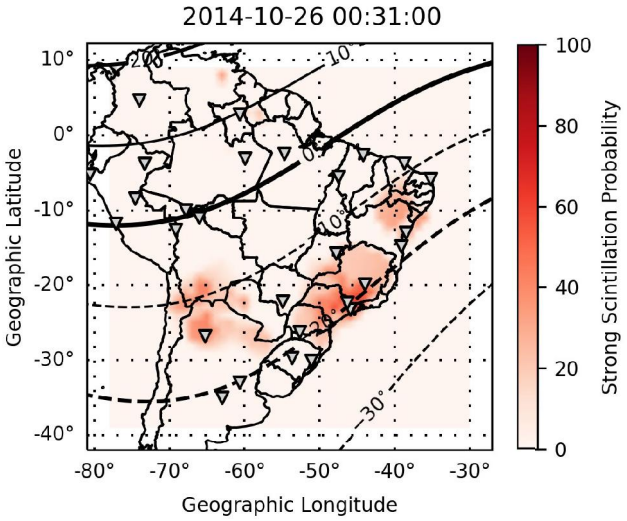

Figure 3. Corresponding strong scintillation probability map, where color scale refers to strong scintillation probability. Curved lines depict magnetic latitudes, and triangles show GPS stations

These scintillation probability maps are intended to evaluate for a user with a GPS receiver on ground or in a vehicle (car, plane, boat, etc.) the risk of suffering a loss-of-lock that may preclude the receiver from acquiring an updated or correct geographic position.

4. Results and Discussion

The proposed probability map approach was evaluated for a set of 40 (15-minute) intervals from November, 2013 to November, 2014, which were selected as presenting strong scintillation over the Brazilian territory. Previously, the corresponding 40 scintillation maps were made using an also newly proposed methodology for pre-processing and interpolation, employed here. Six pre-processing options were tested, combining operators to reduce S4 values for grouped IPPs (using mean, max, or 3rd quartile), and the use of slant or vertically-projected S4 values. The scintillation probability maps were then derived for the strong scintillation level and, for each GPS station, the specific probability was obtained by interpolating the closest four grid points of the probability map. Several error metrics were calculated using the real set of S4 values from all the IPPs of all GPS stations. Considering the four scintillation classes described in the beginning of the former section, a simple count of the number of IPPs of each scintillation class for each station divided by the total of IPPs yields 4 real station-linked ratios for the complete data set, but only the strong level one matters here, being named true strong-class ratio for each station, and composing a set of true strong-class ratios.

In order to evaluate the use of standard scintillation maps, another set of strong-class ratios was calculated for all stations, for the same real IPP positions for each of the 40 intervals, but using the S4 values interpolated directly from the scintillation map, instead of the set of real values. This approximate set of strong-class ratios is named baseline set, likely rendering the lower possible error compared to the true set, also for each pre-processing option employed to produce the scintillation maps. Please note that the scintillation map will provide a GNSS station with a S4 value for its position that is certainly far less accurate than the corresponding one in the baseline set.

The proposed probability map for the considered time interval allows to interpolate the four nearest neighboring grid points to obtain a probability at a given

station for any scintillation class. Considering the strong scintillation class, such probability is equivalent to the true and baseline sets. Finally, the probability and the baseline sets are compared to the corresponding true set for each station. Seven error metrics were employed in the comparison: overall Average (AVG), overall Mean Absolute Error (MAE), overall Root Mean Square Error (RMSE), 40-Mean of Minimum Errors (MIN), 40-Mean of Maximum Errors (MAX), overall Standard Deviation of Absolute Error (STD) and 40-Mean of Pearson's Correlation Coefficient (CORR).

Table 1 shows the error results for the baseline set and for the corresponding values of the proposed probability maps, taking as reference the true set. The best pre-processing options for the baseline set were obtained using the S4 vertical projection and reduction by the mean of the 3rd quartile, while the worst results arose for both slant and vertical S4 values with reduction by the plain mean. Considering the proposed probability maps, the best option was also the S4 vertical projection and reduction by the mean of the 3rd quartile. As expected, errors for the baseline set were lower than for the proposed probability maps, but the latter errors were quite acceptable for a future operational use.

Table 1. Error evaluation for the baseline set of strong-class ratios and the proposed probability maps

ERRORS FOR THE BASELINE SET							
AVG	**MAE**	**RMSE**	**MIN**	**MAX**	**STD**	**CORR**	**OPTIONS**
5.79	6.07	13.11	-2.39	37.62	11.62	0.87	slant_max
-2.03	2.35	5.27	-15.08	3.03	4.71	0.84	slant_mean
3.08	3.75	8.49	-4.58	25.02	7.62	0.92	slant_quantile
5.42	5.75	12.5	-2.56	35.92	11.1	0.87	vertical_max
-2.14	2.41	5.43	-15.53	2.36	4.87	0.83	vertical_mean
2.8	3.51	7.96	-4.83	23.62	7.15	0.91	vertical_quartile
ERRORS FOR THE PROBABILITY MAP							
AVG	**MAE**	**RMSE**	**MIN**	**MAX**	**STD**	**CORR**	**OPTIONS**
12.2	12.25	21.64	-0.67	55.61	17.83	0.78	slant_max
2.93	3.97	8.39	-5.74	24.32	7.39	0.84	slant_mean
9.41	9.5	17.45	-0.98	46.88	14.64	0.81	slant_quantile
5.27	5.77	12.13	-3.87	32.51	10.67	0.84	vertical_max
-2.44	3.05	6.52	-17.43	4.79	5.76	0.74	vertical_mean
2.72	3.72	8.21	-6.09	22.46	7.31	0.87	vertical_quartile

The innovative scintillation probability maps were evaluated using an extensive amount of real S4 index data obtaining low errors according to some metrics, showing the potential of the approach as a real warning tool for strong scintillation in GNSS applications, and also remote sensing and telecommunication satellites in general that employ electromagnetic bands that can be affected by scintillation.

Further works devise the making of scintillation and scintillation probability maps employing multi-constellation GNSS data, instead of only GPS data. Additionally, a specific pre-processing for S4 index missing data due to station technical issues or

loss-of-lock is also intended. Preliminary evaluations already show that real time data acquisition and processing for scintillation and scintillation probability maps making for operational purposes is feasible using standard computational and network resources.

References

de Paula, E. R., Martinon, A. R. F., Moraes, A. O., Carrano, C., Neto, A. C., Doherty, P., et al. (2021). Performance of 6 different global navigation satellite system receivers at low latitude under moderate and strong scintillation. Earth and Space Science, 8, e2020EA001314. https://doi.org/10.1029/2020EA001314

Martinon, A. R. F., Stephany, S. and de Paula, E. R. (2022). Challenges in Real-Time Generation of Scintillation Index Maps. Submitted to the XII Colóquio Brasileiro de Ciências Geodésicas/V Simpósio Brasileiro de Geomática, November 2022, Curitiba/PR - Brazil.

Prol, F. S., Camargo, P. O. and Muella, M. T. A. H. (2017). Comparative Study of Methods for Calculating Ionospheric Points and Describing the GNSS Signal Path. Boletim de Ciências Geodésicas. 2017, v. 23, n. 4, pp. 669-683, ISSN 1982-2170. https://doi.org/10.1590/S1982-21702017000400044.

Rezende, L. F. C., de Paula, E. R., Kantor, I. J. and Kintner, P. M. (2007). Mapping and survey of plasma bubbles over Brazilian territory. The Journal of Navigation, 60(1), 69– 81.

Sato, H., Kim, J. S., Otsuka, Y., Wrasse, C. M., Rodrigues de Paula, E., and Rodrigues de Souza, J. (2021). L-band Synthetic Aperture Radar observation of ionospheric density irregularities at equatorial plasma depletion region. Geophysical Research Letters, 48, e2021GL093541. https://doi.org/10.1029/2021GL093541

Spogli, L., Alfonsi, L., de Franceschi, G., Romano, V., Aquino, M. H. O. and Dodson, A. (2009). Climatology of GPS ionospheric scintillations over high and mid-latitude European regions. Ann. Geophys 27, 3429–3437.

Spogli, L., Alfonsi, L., Romano, V., de Franceschi, G., Monico, G., Shimabukuro, M., Bougar, B. and Aquino M. (2013). Assessing the GNSS scintillation climate over Brazil under increasing solar activity. Journal of Atmospheric and Solar-Terrestrial Physics. s 105–106. 199–206. https://doi.org/10.1016/j.jastp.2013.10.003.

Valladares, C. E. and Chau, J. L. (2012). The low-latitude ionosphere sensor network: Initial results. Radio Science, 47(04), 1-18.

Van Dierendonck, A. J., Klobuchar, J. and Hua, Q. (1993). Ionospheric scintillation monitoring using commercial single frequency C/A code receivers. Paper presented at Proceedings of ION GPS-93, Salt Lake City, UT., 1333-1342.

Vani, B. C., Shimabukuro, M. H., and Monico, J. F. G. (2017). Visual exploration and analysis of ionospheric scintillation monitoring data: the ISMR query tool. Computers & Geosciences, 104, 125-134.